Research Article
Hepatic and Biliary Cancer

JOURNAL
OF HEPATOLOGY

Single-cell RNA sequencing-derived signatures define response patterns to atezolizumab + bevacizumab in advanced hepatocellular carcinoma

Authors

Sarah Cappuyns, Marta Piqué-Gili, Roger Esteban-Fabró, …, Augusto Villanueva, Jeroen Dekervel, Josep M. Llovet

Correspondence

josep.llovet@mountsinai.org (J.M. Llovet), jeroen.dekervel@uzleuven.be (J. Dekervel).

Graphical abstract

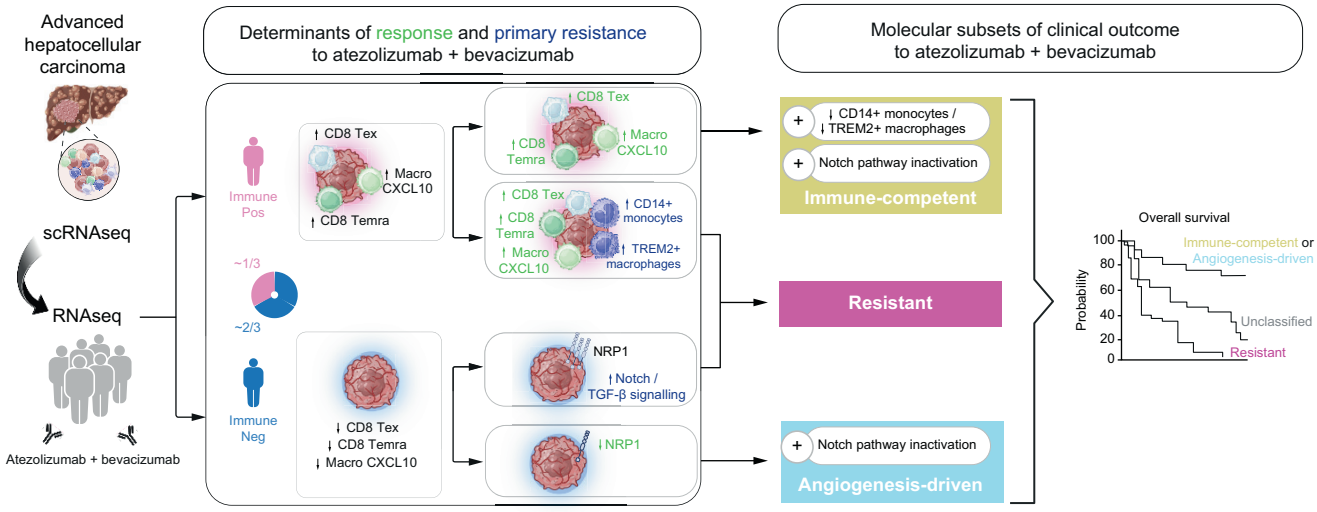

Highlights

- Single-cell-derived gene signatures were identified for 21 cell types in the advanced HCC TME.
- Response to atezo+bev is driven by two distinct mechanisms: immune-*vs.* angiogenesis-driven.
- Immunosuppressive myeloid cells and Notch activation contribute to treatment resistance.
- Molecular stratification determines clinical outcomes with atezo+bev in advanced HCC.

Impact and implications

Atezolizumab + bevacizumab (atezo+bev) is standard of care in advanced hepatocellular carcinoma (HCC), yet molecular determinants of clinical benefit to the combination remain unclear. This study harnesses the power of single-cell RNA sequencing, deriving gene expression signatures representing 21 cell subtypes in the advanced HCC microenvironment. By applying these signatures to RNA-sequencing samples, we reveal two distinct response patterns to atezo+bev and define molecular subgroups of patients (“*Immune-competent”* and “*Angiogenesis-driven” vs*. *“Resistant”*) with differential clinical outcomes upon treatment with atezo+bev, pointing towards the role of immunosuppressive myeloid cell types and Notch pathway activation in primary resistance to atezo+bev. These results may help refine treatment strategies and improve outcomes for patients with advanced HCC, while also guiding future research aimed at overcoming resistance mechanisms.

https://doi.org/10.1016/j.jhep.2024.12.016
 J. Hepatol. 2025, 82, 1036–1049

Research Article
Hepatic and Biliary Cancer

JOURNAL
OF HEPATOLOGY

Single-cell RNA sequencing-derived signatures define response patterns to atezolizumab + bevacizumab in advanced hepatocellular carcinoma

Sarah Cappuyns[1,2,3,4,5,†], **Marta Piqué-Gili**[5,6,†], **Roger Esteban-Fabró**[5,6,†], Gino Philips[3,4], Ugne Balaseviciute[6], Roser Pinyol[6], Albert Gris-Oliver[6], Vincent Vandecaveye[7,8], Jordi Abril-Fornaguera[5,6], Carla Montironi[6,9], Laia Bassaganyas[10], Judit Peix[6], Marcus Zeitlhoefler[5], Agavni Mesropian[5,6], Júlia Huguet-Pradell[5,6], Philipp K. Haber[11], Igor Figueiredo[12], Giorgio Ioannou[12], Edgar Gonzalez-Kozlova[12], Antonio D'Alessio[13], Raphael Mohr[14], Tim Meyer[15], Anja Lachenmayer[16], Jens U. Marquardt[17], Helen L. Reeves[18,19], Julien Edeline[20], Fabian Finkelmeier[21], Jörg Trojan[21], Peter R. Galle[22], Friedrich Foerster[22], Beatriz Mínguez[23,24,25], Robert Montal[26], Sacha Gnjatic[12], David J. Pinato[13,27], Mathias Heikenwalder[28], Chris Verslype[1,2], Eric Van Cutsem[1,2], Diether Lambrechts[3,4], Augusto Villanueva[5], Jeroen Dekervel[1,2,*,‡], Josep M. Llovet[5,6,29,*,‡]

Journal of Hepatology **2025**. vol. 82 | 1036–1049

Background & Aims: The combination of atezolizumab and bevacizumab (atezo+bev) is the current standard of care for advanced hepatocellular carcinoma (HCC), providing a median overall survival (OS) of 19.2 months. Here, we aim to uncover the underlying cellular processes driving clinical benefit *vs.* resistance to atezo+bev.

Methods: We harnessed the power of single-cell RNA sequencing in advanced HCC to derive gene expression signatures recapitulating 21 cell phenotypes. These signatures were applied to 422 RNA-sequencing samples of patients with advanced HCC treated with atezo+bev (n = 317) *vs*. atezolizumab (n = 47) or sorafenib (n = 58) as comparators.

Results: We unveiled two distinct patterns of response to atezo+bev. First, an immune-mediated response characterised by the combined presence of CD8+ T effector cells and pro-inflammatory CXCL10+ macrophages, representing an immune-rich microenvironment. Second, a non-immune, angiogenesis-related response distinguishable by a reduced expression of the VEGF co-receptor neuropilin-1 (*NRP1*), a biomarker that specifically predicts improved OS upon atezo+bev *vs*. sorafenib (p = 0.039). Primary resistance was associated with an enrichment of immunosuppressive myeloid populations, namely CD14+ monocytes and TREM2+ macrophages, and Notch pathway activation. Based on these mechanistic insights we define "*Immune-competent*" and "*Angiogenesis-driven*" molecular subgroups, each associated with a significantly longer OS with atezo+bev *vs.* sorafenib (p of interaction = 0.027), and a "*Resistant*" subset.

Conclusion: Our study unveils two distinct molecular subsets of clinical benefit to atezolizumab plus bevacizumab in advanced HCC ("*Immune-competent*" and "*Angiogenesis-driven*") as well as the main traits of primary resistance to this therapy, thus providing a molecular framework to stratify patients based on clinical outcome and guiding potential strategies to overcome resistance.

Introduction

Hepatocellular carcinoma (HCC) is the third leading cause of cancer-related mortality worldwide,[1] and incidence rates are rising rapidly. Approximately 50-60% of patients with HCC eventually evolve to advanced stages of the disease requiring systemic therapies.[2] In 2020, the combination of atezolizumab, an anti-PDL1 immune checkpoint inhibitor (ICI), and bevacizumab, a VEGFA inhibitor (hereafter, atezo+bev), was shown to significantly improve survival compared to sorafenib, the standard of care for over a decade,[3] in the IMbrave150 phase III randomised study (19.2 *vs*. 13.4 months).[4,5] Thus, atezo+bev was established as the new standard of care in advanced HCC, achieving an objective response in ~35% of patients. However, the molecular determinants of clinical benefit from the combination are yet to be robustly defined.[6–8]

The tumour microenvironment (TME) plays a crucial role in HCC development and progression, mediating response and/or resistance to immunotherapy.[7,9] Several gene expression

* Corresponding authors. Addresses: Mount Sinai Liver Cancer Program, Division of Liver Diseases, Tisch Cancer Institute, Icahn School of Medicine at Mount Sinai, New York, NY, USA. (J.M. Llovet), or Digestive Oncology, Department of Gastroenterology and Hepatology, UZ/KU Leuven, Belgium. (J. Dekervel).
E-mail addresses: josep.llovet@mountsinai.org (J.M. Llovet), jeroen.dekervel@uzleuven.be (J. Dekervel).
† Shared first authors are denoted in bold.
‡ Shared senior authorship.
https://doi.org/10.1016/j.jhep.2024.12.016

signatures that recapitulate inflamed classes of HCC or inflammatory signalling have been associated with response to single-agent anti-PD1.[10–14] Consistently, pre-existing tumour immunity – namely high PD-L1 expression, a T-effector signature[15] and high intra-tumoural CD8+ T-cell density – was associated with better clinical outcomes in atezo+bev-treated patients, and an "atezo+bev response signature" was derived.[6] However, a general issue when generating genomic signatures is the lack of biological insights or mechanistic rationale that links selected genes with outcome. Consequently, so far, none of these gene signatures have made it to clinically validated biomarkers of response to systemic therapy in advanced HCC.[8]

Recent advances in single-cell RNA sequencing (scRNAseq) have become key to study phenotypical and functional diversity of tumour-infiltrating stromal and immune cells, allowing for the exploration of the TME of advanced HCC and how it relates to ICI response.[16–18] However, single-cell sequencing technologies are not suitable for use in routine clinical practice.

Here, using scRNAseq data of 31 advanced HCC tumours, we generate cell type-specific gene signatures representing 21 distinct cell phenotypes. We then explore their potential as predictive biomarkers of atezo+bev response using bulk transcriptomic data from 422 pre-treatment advanced HCC samples. We unveil two distinct subtypes of responders to atezo+bev: a first subgroup is defined by the combined intratumoural presence of two CD8+ effector T-cell subtypes and CXCL10+ macrophages, representing an immune-rich TME, while a second subgroup of responders lacks infiltration by these three immune-related cell types and is distinguished by a reduced expression of the VEGF co-receptor neuropilin-1 (*NRP1*). Moreover, we highlight the role of immunosuppressive cells and Notch activation in primary resistance to atezo+bev. Finally, patients were categorized accordingly into molecular subsets predictive of clinical benefit or resistance to atezo+bev.

Materials and methods

Study design

We aimed to leverage the single-cell resolution offered by scRNAseq technologies to generate gene signatures that can be applied to RNAseq data analysis (Fig. 1). We first used scRNAseq data to generate gene signatures representative of the cellular heterogeneity present in the TME of advanced HCC.[17] These gene signatures were then applied to RNAseq cohorts to identify response subtypes and determinants of response *vs.* resistance to atezo+bev.

Patient cohorts and sample collection

This study encompasses six cohorts. An overview is provided in Table S1 (see supplementary methods for details).

The scRNAseq discovery cohort[17] and scRNAseq validation cohort[18] include a total of 47 advanced HCC tumours, taken prior to the start of systemic treatment. Samples were subjected to scRNAseq and used to generate and validate scRNAseq-derived gene signatures.

The in-house RNAseq cohort and the external RNAseq cohort[6] comprise a total of 422 pre-treatment HCC tumour samples subjected to RNAseq. Patients were treated with atezo+bev (n = 317), atezolizumab (n = 47) or sorafenib (n = 58) and stratified into responders *vs.* non-responders according to best objective response.[19] Responders displayed either complete or partial response, while non-responders were defined as those patients with stable disease (SD) or progressive disease (PD). Disease control comprises complete or partial response, or SD as best response. Secondary endpoints were overall survival (OS) and progression-free survival (PFS). See Fig. S1 for details.

The external whole-exome sequencing (WES) cohort[6] and the anti-PD1 validation cohort[10] are described in the supplementary methods.

Generating scRNAseq-derived gene signatures

Using a tailored bioinformatics pipeline, adapted from a previous study,[20] we generated scRNAseq-derived gene signatures for the 35 cell (pheno-)types identified at the single-cell resolution in the scRNAseq discovery cohort.[17] Starting from the fully annotated single-cell dataset, we performed differential gene expression analysis to identify differentially expressed genes (DEGs) for each cell (pheno-)type using the *FindAllMarkers* function from Seurat 4.[21] DEGs were selected based on the Wilcoxon rank sum test, restricted to genes expressed in at least 10% of cells. Ribosomal, mitochondrial and immunoglobulin genes were removed and only genes with average log2-fold change ≥1.5 were selected, hypothesizing that DEGs above this threshold would be captured in RNAseq data.

To generate cell type-specific gene signatures, we further filtered the resulting list of up-*vs.* downregulated DEGs, separately. An overview is provided in Fig. S2A. Please refer to supplementary methods for details on DEG filtering steps and signature categorization as specific or not specific.

In sum, we generated 'specific' gene signatures to identify 21 distinct cell (pheno-)types present in the TME of advanced HCC (Fig. 2B and Fig. S3). An overview of the scRNAseq-derived gene signatures is provided in Table S2.

For details on the characterisation and validation of the scRNAseq-derived gene signatures, as well as the analysis and statistics of bulk transcriptomics, genomic WES data, experimental models of HCC, flow cytometry and multiplexed immunohistochemistry data, please refer to the supplementary methods.

Definition of molecular subsets of atezo+bev clinical outcome

Patients from the external RNAseq cohort treated with atezo+bev were categorized according to the presence or absence of the scRNAseq-derived gene signatures recapitulating CD8 Temra, CD8 Tex, Macro CXCL10, TREM2+ macrophage and CD14+ monocyte immune populations, as well as into having Notch pathway activation *vs*. inactivation based on a previously reported signature in HCC.[22] Additionally, patients were classified as NRP1-Low if tumour NRP1 expression was ≤0.75 of the mean in adjacent liver tissue, and as NRP1-High otherwise. For details on the classification criteria into *"Immune-competent"*, "*Angiogenesis-driven*" and *"Resistant"* molecular subsets, please refer to the supplementary methods.

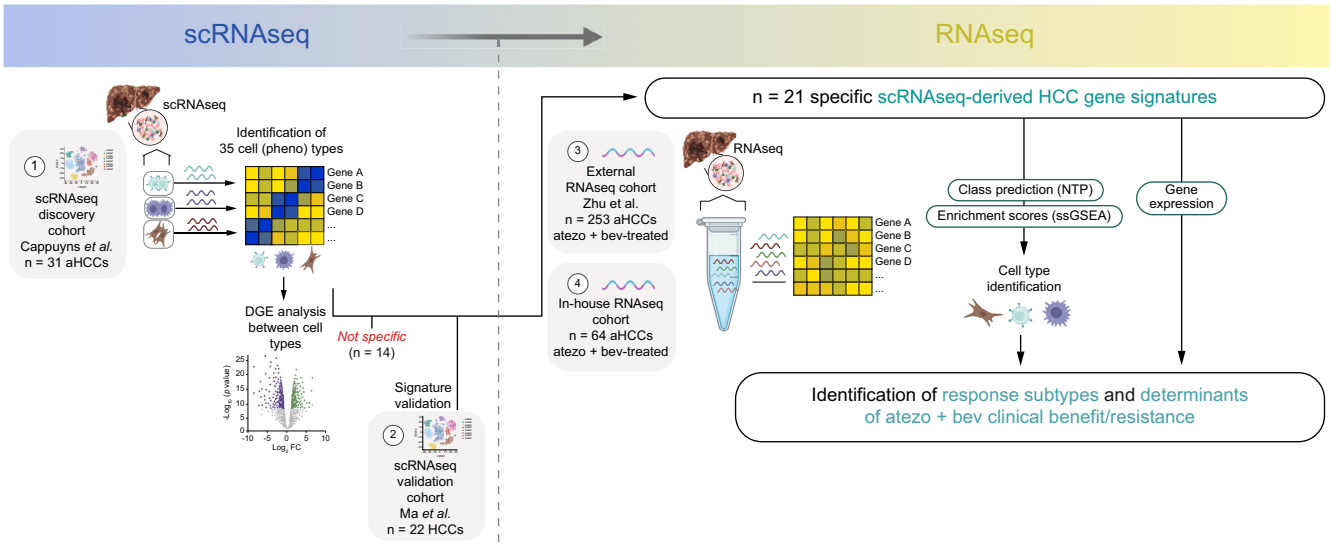

Fig. 1. Study design. aHCC, advanced hepatocellular carcinoma; atezo+bev, atezolizumab + bevacizumab; DGE, differential gene expression; RNAseq, bulk RNA sequencing; scRNAseq, single-cell RNA sequencing; ssGSEA, single-sample gene set-enrichment analysis.

Results

Generation of specific, robust and biologically plausible gene signatures capturing cell phenotypes identified from scRNAseq in advanced HCC

Here, we aimed to leverage the single-cell resolution offered by scRNAseq technologies to generate gene signatures that are applicable to conventional RNAseq data analysis, a more widely available technique. Thus, these gene signatures could enable the assessment of cellular heterogeneity and lead to informed clinical decision-making.

First, we aimed to generate scRNAseq-derived gene signatures representative of the cellular heterogeneity present in the TME of advanced HCC.[17] Using scRNAseq data from advanced HCC tumours (91,347 cells; scRNAseq discovery cohort) and a tailored-bioinformatics pipeline (Fig. 1 and Fig. S2A), we generated gene signatures for 35 cell (pheno-) types[17] (Fig. 2A), including malignant hepatocytes as well as immune and stromal cell types. Each scRNAseq-derived HCC gene signature consisted of a comparable number of genes, with an average of 36 upregulated (range 8-110 genes) and 30 downregulated genes (range 7-125 genes; Fig. S2B; Table S2). We then evaluated the specificity, robustness, and biological relevance of the resulting HCC gene signatures. To assess the specificity, each signature was categorized as specific or not specific according to its combined expression score per cell (see supplementary methods for details; Fig. S3 for clarity), and we found 21 of the HCC gene signatures to be specific for their intended cell type (Fig. 2B). Gene signatures predicting myeloid subtypes generally performed better than those predicting T-cell phenotypes (Fig. 2B and Fig. S3), likely due to the higher degree of transcriptomic similarity between distinct T-cell phenotypes. Non-specific signatures were discarded for further downstream analyses. Signature robustness was evaluated using an independent, publicly available scRNAseq cohort of 22 predominantly viral HCCs (n = 45.477 single cells; scRNAseq validation cohort).[18] Firstly, among the 35 cell types identified in the scRNAseq discovery cohort, 31 were also present in the scRNAseq validation cohort (Figs. S4A–C). Secondly, the HCC gene signatures deemed as specific identified the same cell types in both the scRNAseq discovery and validation cohorts, confirming the robustness of our methodology (Fig. 2C). The biological plausibility of each signature, *i.e.* that the genes comprising each signature were coherent with the corresponding cell phenotype and function, was confirmed using Enrichr (Fig. 2D).[23] Taken together, out of the 35 malignant, immune and stromal cell types identified in the TME of advanced HCC using scRNAseq, we generated 21 specific, robust and biologically plausible scRNAseq-derived gene signatures that accurately represent the intra-tumoural cellular heterogeneity of advanced HCC.

scRNAseq-derived HCC gene signatures and response to atezo+bev in advanced HCC

Next, we used the HCC gene signatures to dissect the intra-tumoural cell type composition of patients with advanced HCC using two bulk RNAseq cohorts, comprising samples from a total of 422 patients treated with atezo+bev (n = 317), atezolizumab (n = 47) or sorafenib (n = 58). We aimed to explore the potential of these signatures as predictors of response to atezo+bev, given that the intra-tumoural presence of specific cell types has previously been linked to response and/or resistance to therapy.[17]

Firstly, we collected tumour tissue samples from 96 patients with advanced HCC treated with atezo+bev, of whom 71 were subjected to RNAseq (in-house RNAseq cohort; Fig. S1A) and 64 remained after quality control filtering. An overview of patient and tumour characteristics is provided in Table S3. The objective response rate to atezo+bev was 31% (consistent with results from IMbrave150[4,5]; Fig. S1A), median follow-up was 20 months, and median OS (mOS) was 14 months. As expected, patients responding to atezo+bev had significantly longer mOS and median PFS compared to non-responders (Fig. S1B).

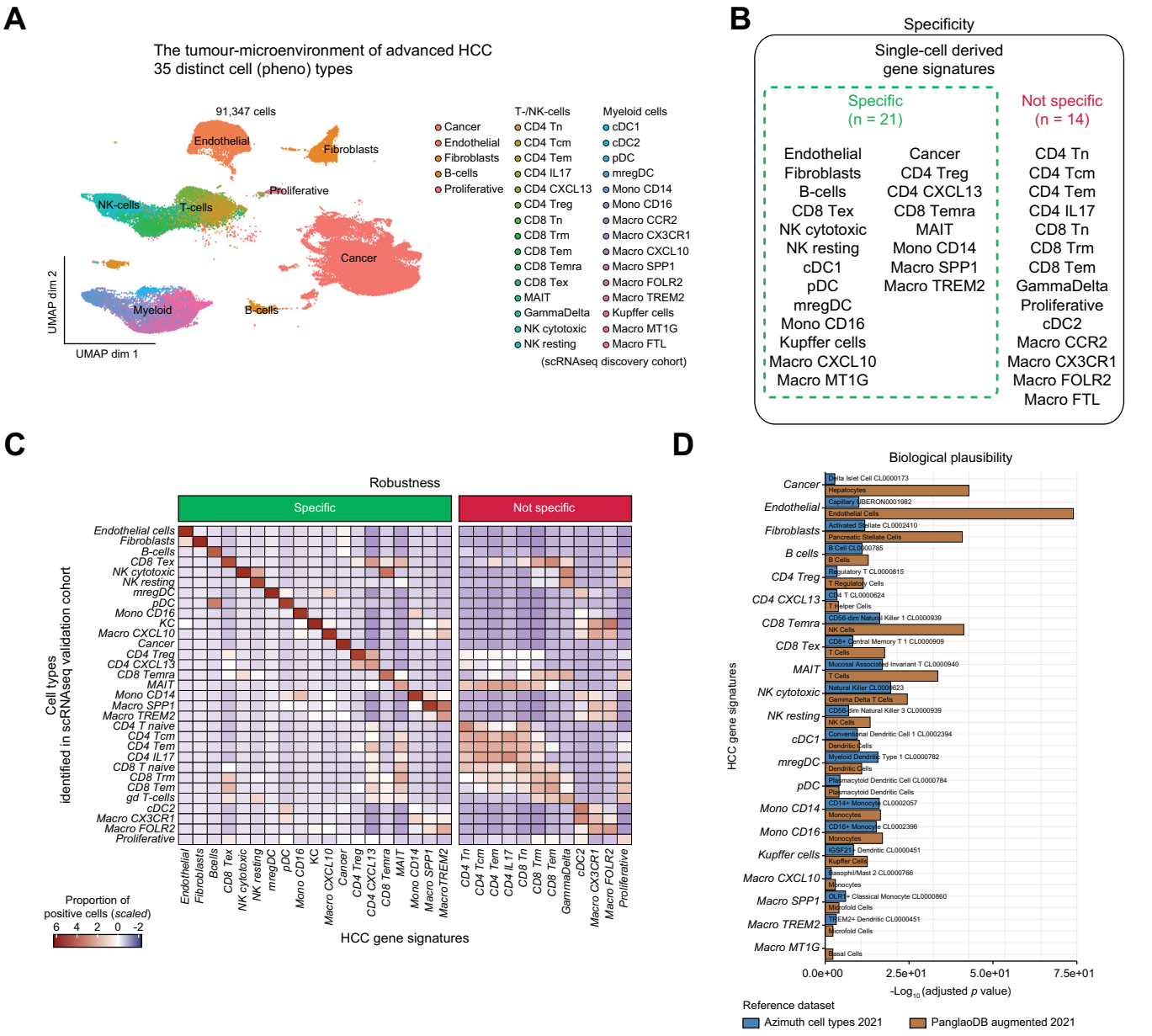

Fig. 2. Identification of specific, robust and biologically plausible single cell-derived HCC gene signatures. (A) UMAP representation of the 35 cell types identified in the TME. (B) Overview of HCC gene signatures generated in this study. (C) Heatmap of the proportion of cells positive for each HCC gene signature, calculated in each cell type, stratified according to signature specificity. (D) Barplot depicting the top cell types identified for each specific HCC gene signature (n = 21) in two single-cell reference datasets, ranked according to adjusted *p* values. HCC, hepatocellular carcinoma; UMAP, uniform manifold approximation and projection.

A second publicly available RNAseq cohort (external RNA-seq cohort) consisting of prospectively collected pre-treatment tumour biopsies of patients with advanced HCC treated in the context of the phase Ib (GO30140) and phase III (IMbrave150) trials was used.[4–6,24] Of the 247 patients treated with atezo+bev with available response data, 81 were responders (objective response rate = 33%; Fig. S1C). All tissue samples in the external RNAseq cohort were collected a maximum of 12 months prior to the start of systemic therapy. To maximize the comparability between the two cohorts, we focused our analyses on those samples from the in-house RNAseq cohort that were collected within 12 months of starting atezo+bev treatment (n = 39; 11 responders *vs.* 28 non-responders).

To explore the potential value of our generated scRNAseq-derived HCC gene signatures in predicting clinical response to atezo+bev, we calculated enrichment scores per sample for each gene signature (Fig. 3A and Fig. S5A). In line with previous findings,[17] three cell types, namely two types of CD8+ effector cells (CD8 Temra, CD8 Tex) and pro-inflammatory CXCL10+ macrophages (Macro CXCL10), were consistently enriched in atezo+bev responders compared to non-responders in both RNAseq cohorts (Fig. 3B and Fig. S5B). Individually, these three signatures identified responders with areas under the curve ranging from 0.63 to 0.79 (Fig. 3B and Fig. S5B). Notably, the presence of each of the three immune-related signatures was associated with significantly longer PFS upon treatment with

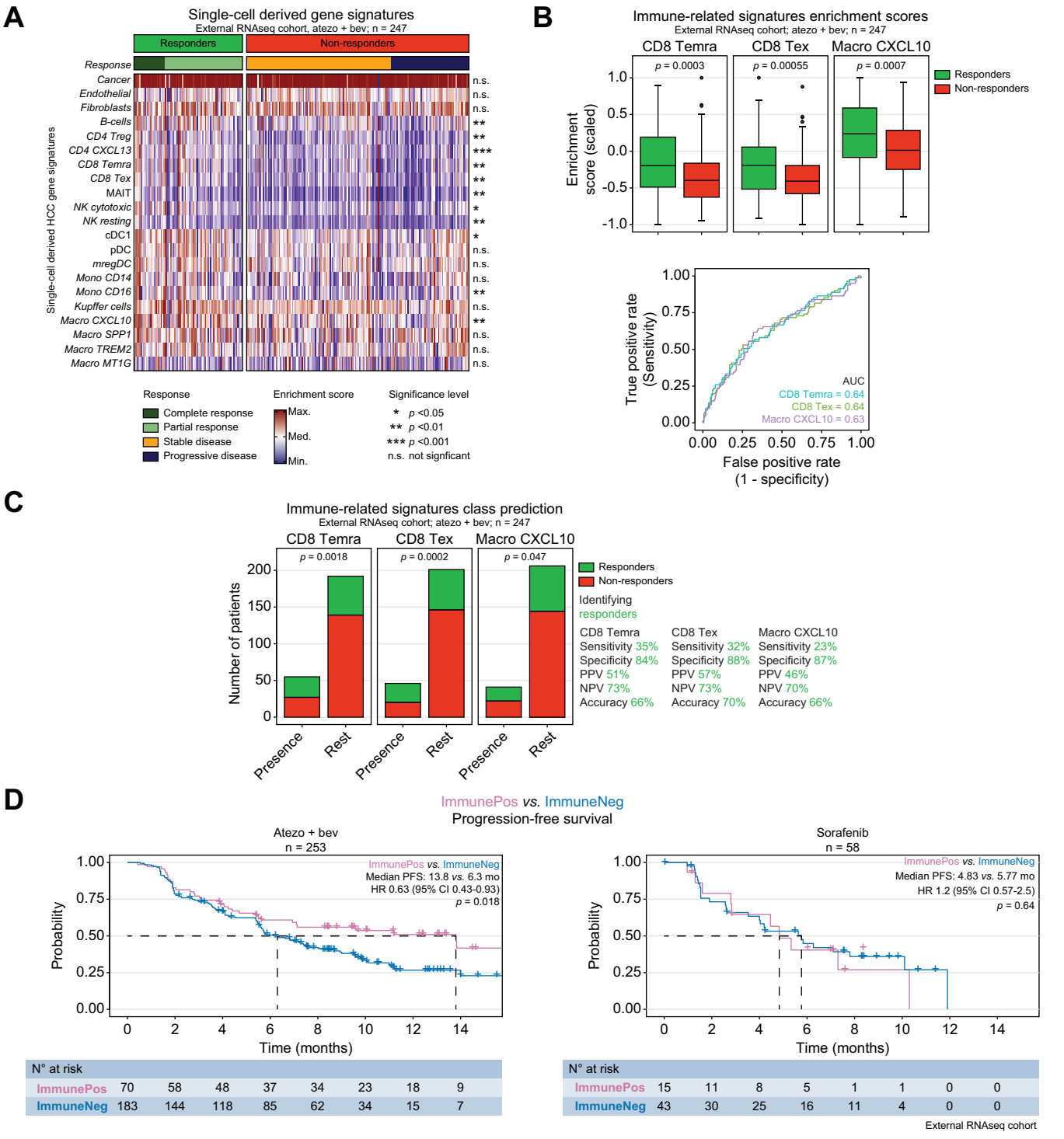

Fig. 3. Single cell-derived HCC gene signatures and response to atezo+bev. (A) Heatmap depicting the enrichment of HCC gene signatures in each sample, stratified for response to atezo+bev. (B) *Top*: Boxplots depicting enrichment scores of CD8 Temra, CD8 Tex and Macro CXCL10, stratified for response to atezo+bev. *Bottom*: Receiver-operating characteristic curves showing the performance of each signature in predicting response to atezo+bev. AUC as indicated. (C) *Left:* Barplot depicting the presence of CD8 Temra, CD8 Tex and Macro CXCL10 in the TME, coloured for response to atezo+bev. *Right*: Sensitivity, specificity, PPV, NPV, and accuracy of response detection based on the presence of CD8 Temra, CD8 Tex and Macro CXCL10. (D) Kaplan-Meier curves depicting PFS of *ImmunePos vs. ImmuneNeg* tumours in patients treated with atezo+bev (n = 253, *left*) *vs.* sorafenib (n = 58, *right*). Statistics: A-B: Student's *t* test, Welch's t-test or Wilcoxon rank sum test, as appropriate. C: Fisher's exact test. D: HR, 95% CIs and *p* values calculated using a univariate cox regression analysis. Atezo+bev, atezolizumab + bevacizumab; HCC, hepatocellular carcinoma; HR, hazard ratio; NPV, negative predictive value; PFS, progression-free survival; PPV, positive predictive value; TME, tumour microenvironment.

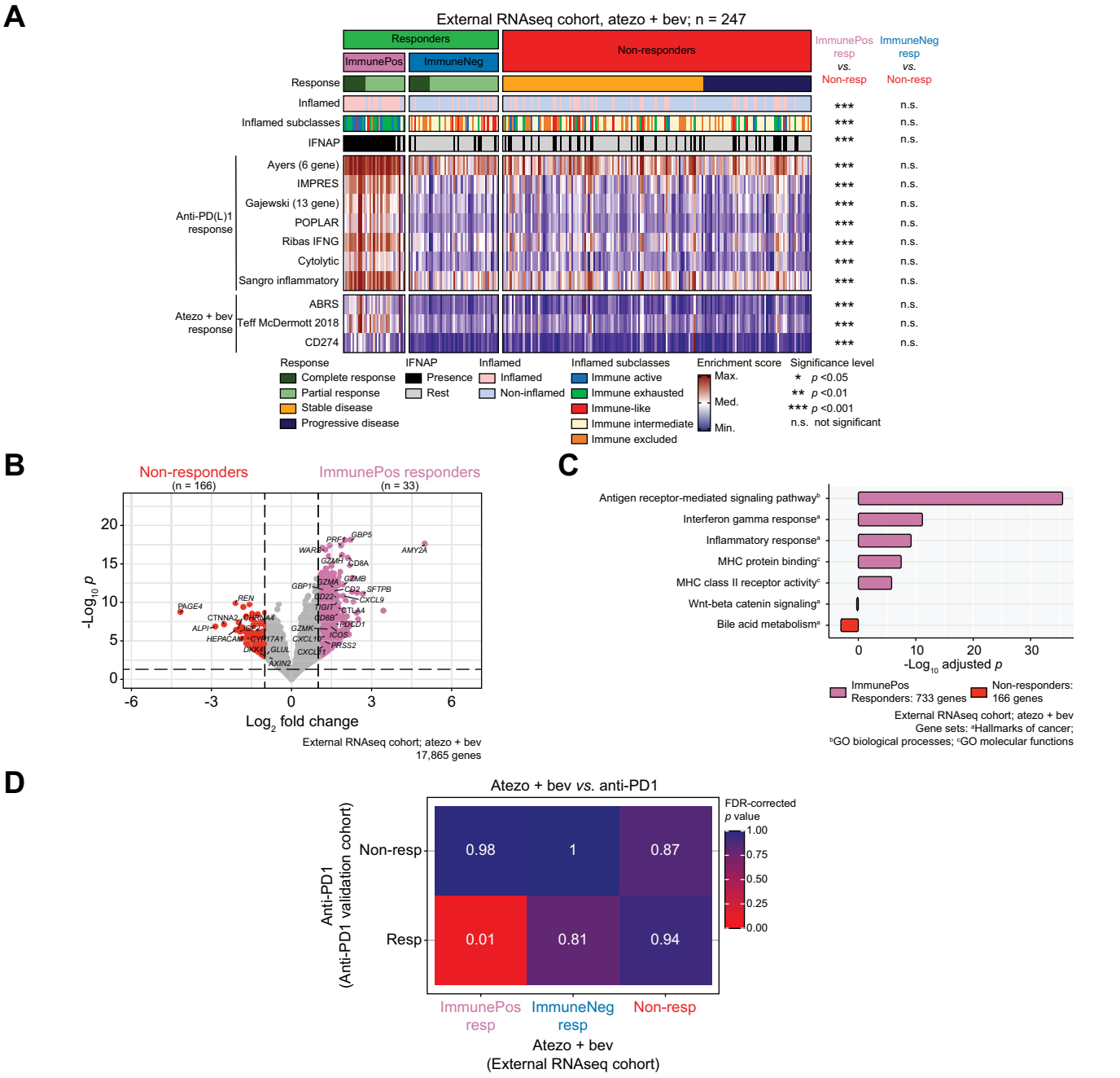

Fig. 4. Immune-mediated response to atezo+bev in advanced HCC. (A) Heatmap representation of HCC inflamed (sub)classes and gene signatures previously associated with response to anti-PD(L)1 monotherapy in *ImmunePos* and *ImmuneNeg* responders *vs.* non-responders to atezo+bev. (B) Volcano plot depicting differentially expressed genes between *ImmunePos* responders (n = 33) and non-responders (n = 166) to atezo+bev. (C) Pathways enriched based on differentially upregulated genes in *ImmunePos* responders (n = 733 genes) *vs.* non-responders to atezo+bev (n = 166 genes), identified in Fig. 4B. (D) SubMap analysis evaluating transcriptomic similarity between response groups in atezo+bev-*vs.* anti-PD1-treated patients. FDR-corrected *p* values are shown. Statistics A: Student's *t* test, Welch's t-test, Wilcoxon rank sum test or Fisher's exact test, as appropriate. Atezo+bev, atezolizumab + bevacizumab; FDR, false discovery rate; HCC, hepatocellular carcinoma; RNAseq, bulk RNA sequencing.

atezo+bev, specifically in the external RNAseq cohort (Fig. S5C), an association that was not observed with other cell types enriched in responders. The CD8 Temra, CD8 Tex and Macro CXCL10 signatures identified atezo+bev responders with a specificity of 84%-88% (Fig. 3C), though their sensitivity was low in both cohorts (Fig. 3C; Fig. S5D).

Importantly, the three immune-related signatures were strongly correlated (Fig. S6A and B), suggesting the coexistence of these cell types in the advanced HCC TME. Hence, we classified tumours positive for at least one of the three immune-related signatures as immune-positive tumours (*ImmunePos*), while cases negative for all three immune-related signatures

were categorized as immune-negative (*ImmuneNeg*). Compared to *ImmuneNeg* cases, *ImmunePos* tumours were associated with a significantly longer PFS upon treatment with atezo+bev (median PFS 11.1 *vs*. 5.9 months; hazard ratio 0.62; 95% CI 0.43-0.90; $p = 0.011$), an association that was not seen in sorafenib-treated patients, supporting the role of an *ImmunePos* status as a predictive biomarker of response to atezo+bev (p of interaction = 0.09; 95% CI 0.234-1.117; Fig. 3D).

Immune- *vs*. non-immune-mediated response to atezo+bev in advanced HCC

In line with the low sensitivity of the *ImmunePos*-defining signatures to identify atezo+bev responders, only 41-55% of responders were classified as *ImmunePos* (33/81 and 6/11 responders in the external and in-house RNAseq cohort, respectively). Importantly, compared to non-responders, *ImmunePos* responders were enriched in the HCC inflamed class ($p < 0.001$)[14] and signatures previously associated with response to anti-PD(L)1 monotherapy in both HCC[10–13] and other cancer types[25–29] (Fig. 4A). In contrast, *ImmuneNeg* responders were immune cold tumours, displaying a degree of inflammation comparable to that observed in non-responding tumours (Fig. 4A), suggesting that distinct mechanisms might underlie response to atezo+bev in *ImmunePos vs. ImmuneNeg* tumours. To explore this, we first used differential gene expression analysis to compare *ImmunePos* atezo+bev responders to all non-responders regardless of immune status. *ImmunePos* responders were enriched in genes associated with CD8 T cells (*CD8A, CD8B*), cytotoxicity (*PRF1, GZMA, GZMB, GZMH*) and interferon-gamma activity (*GBP1, GBP5*), as well as genes involved in T-cell recruitment (*CXCL9/10/11*; Fig. 4B). Additional pathway analysis confirmed the enrichment of immune-related gene sets in *ImmunePos* responders in both the in-house and external RNAseq cohorts (Fig. 4C and Fig. S6C,D). Compared to non-responding tumours, *ImmunePos* responders also exhibited a decrease in the expression of genes related to Wnt-β catenin signalling (*GLUL, AXIN2, DKK4*), previously related to immune cold tumours and ICI monotherapy refractoriness.[30] Furthermore, we compared atezo+bev-treated patients to a cohort of 28 anti-PD1-treated patients with advanced HCC (anti-PD1 validation cohort) using an unsupervised subclass mapping method (SubMap[31]) and found that anti-PD1 responders were most transcriptomically similar to *ImmunePos* atezo+bev responders (Fig. 4D). Taken together, these findings suggest that *ImmunePos* responders may represent tumours more susceptible to the immune-activating effect of anti-PD(L)1 treatment.

Next, we aimed to identify potential response mechanisms in *ImmuneNeg* responders. Compared to non-responders, *ImmuneNeg* responders displayed an enrichment in signalling pathways related to cell cycle, MYC targets, DNA replication and DNA repair (Fig. S6E), suggesting genomic instability. To explore this further, we analysed WES data from 67 patients (external WES cohort). *ImmuneNeg* responders tended to be enriched in copy number alterations (CNAs) involving ≥50% of a chromosome arm, as indicated by higher broad CNA scores, compared to both *ImmunePos* responders and non-responders ($p = 0.16$ and $p = 0.28$; Fig. S7A). Furthermore, the presence of both high broad CNA loads[32] and *TP53* loss-of-heterozygosity was significantly higher in *ImmuneNeg* responders (n = 7/13, 54%) compared to non-responders to atezo+bev (n = 10/43, 23%; $p = 0.046$; Fig. 5A). This supports the notion that *ImmuneNeg* responders include genomically unstable tumours with *TP53* alterations, previously linked to anti-VEGF response in other cancers.[33] Further, it suggests that *ImmuneNeg* responders might be benefitting more from the angiogenesis-related effects of bevacizumab.

As bevacizumab targets the VEGF/VEGFR axis, we assessed the expression levels of the VEGF receptors 1-3 and their ligands (Fig. 5B and Fig. S7B), as well as the VEGF co-receptor neuropilin-1 (*NRP1;* Fig. 5C). *ImmuneNeg* responders presented higher *VEGFA* levels compared to *ImmunePos* responders, although no significant differences were observed *vs*. non-responders (Fig. 5B). Most notably, and in line with our hypothesis that *ImmuneNeg* atezo+bev responders might be more susceptible to anti-VEGFA, we found that *NRP1* expression was significantly lower in this group of patients compared to *ImmunePos* responders and to non-responders (Fig. 5C). Low tumour *NRP1* expression is, in fact, one of the most consistently described intra-tumoural biomarkers for bevacizumab response.[34] Importantly, patients with low *NRP1* tumours had significantly longer PFS and OS upon treatment with atezo+bev (Fig. 5D,E), as opposed to sorafenib (p of interaction for OS = 0.039) or atezolizumab monotherapy (Fig. S7C). Remarkably, in the scRNAseq discovery cohort, we found the highest expression of *NRP1* to be in endothelial cells and pericytes (Fig. 5F).

Taken together, our findings unveil two distinct mechanisms associated with response to atezo+bev: immune-*vs.* non-immune-mediated response. A first subset of atezo+bev responders are characterised by an immune-rich TME with infiltration of CD8 effector cells and pro-inflammatory macrophages and are identifiable using scRNAseq-derived gene signatures that represent these cell types. A second subset of responders present with genomically unstable tumours lacking the necessary anti-tumoural immune component, and characterised by decreased *NRP1* expression.

Targeting NRP1 in combination with anti-PDL1 + anti-VEGFA remodels the anti-tumour immune microenvironment in a resistant murine model of HCC

To explore whether blocking NRP1 could offer a potential strategy for improving atezo+bev responses, we generated an orthotopic HCC murine model by implanting Hep53.4 cells – exhibiting resistance to anti-PDL1 + anti-VEGFA (Fig. S8) – into the livers of C57BL/6J mice (see supplementary methods for details). Animals were treated with (i) vehicle; (ii) anti-PDL1 + anti-VEGFA; (iii) an NRP1 inhibitor (EG00229); or (iv) the triple combination of anti-PDL1 + anti-VEGFA + EG00229 (Fig. S9A). Flow cytometry analysis showed a significant increase in CD8+ T-cell subsets in the triple combination arm compared to vehicle (Fig. S9B), an effect not observed with anti-PDL1 + anti-VEGFA alone. Additionally, tumours from mice treated with anti-PDL1 + anti-VEGFA + EG00229 presented a higher CD8+/regulatory T-cell ratio compared to vehicle ($p = 0.015$) and to anti-PDL1 + anti-VEGFA ($p = 0.098$) arms (Fig. S9C). Overall, these results indicate that targeting NRP1 in combination with anti-PDL1 + anti-VEGFA results in a more favourable anti-tumour immune profile, consistent with previous reports in preclinical melanoma models.[35]

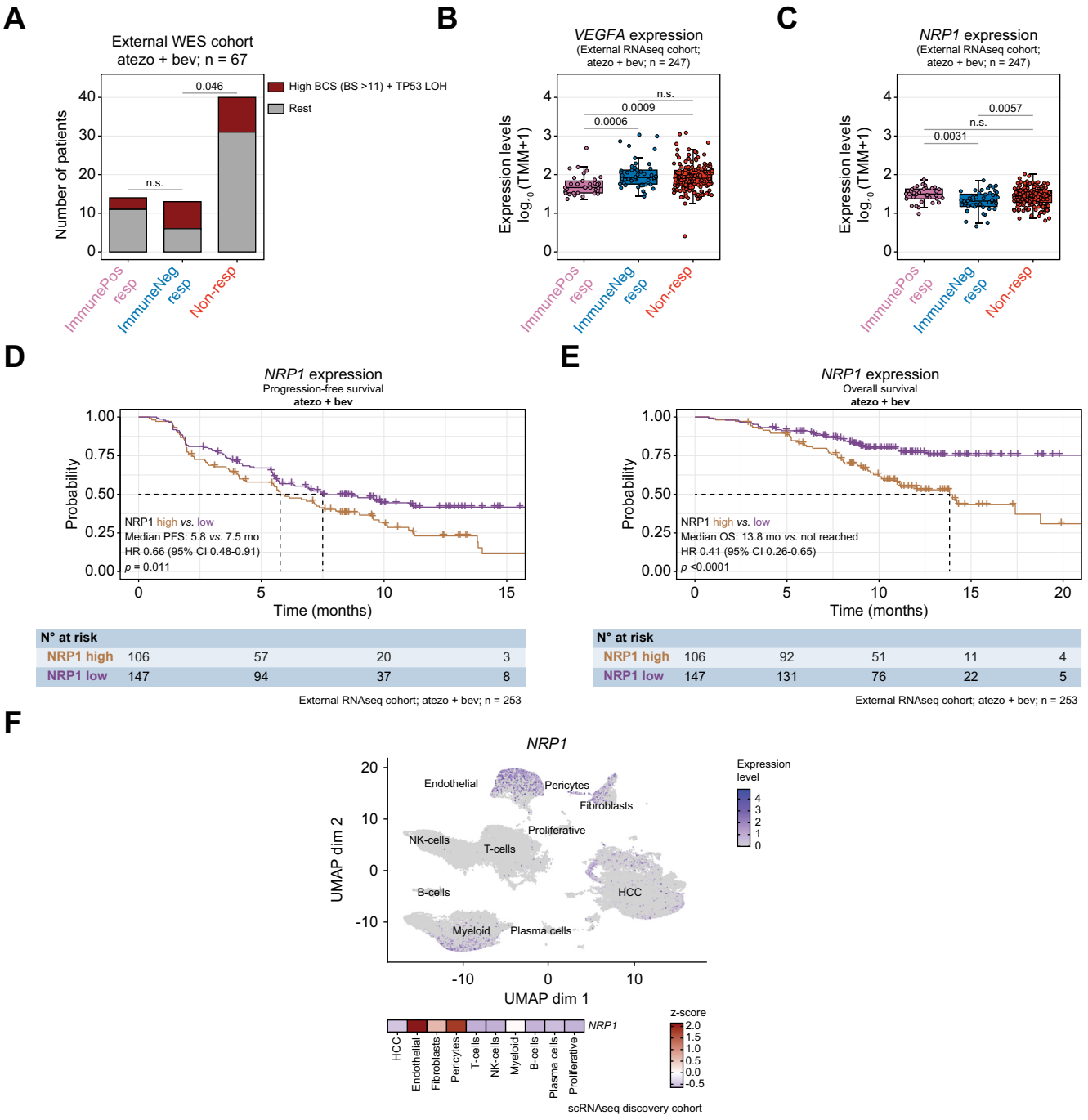

Fig. 5. Angiogenesis-related response to atezo+bev in advanced HCC. (A) Barplot representing the number of patients presenting both high broad Copy Number Alteration (CNA) loads and *TP53* loss of heterozygosity across response subgroups. (B) Boxplots depicting *VEGFA* expression levels across atezo+bev response groups. (C) Boxplots depicting *NRP1* expression levels across atezo+bev response groups. (D) Kaplan-Meier curves depicting PFS of atezo+bev-treated patients (n = 253) according to low *NRP1* expression status. (E) Kaplan-Meier curves depicting OS of atezo+bev-treated patients (n = 253) according to low *NRP1* expression status. (F) *Top*: UMAP representation of *NRP1* expression in the TME. *Bottom*: Heatmap of *NRP1* expression in each cell type identified in the TME. Statistics: A: Fisher's exact test; B–C: Kruskal-Wallis test followed by Dunn-test adjusted by Benjamini-Hochberg. E-F: HR, 95% CI and *p* values calculated using a univariate cox regression analysis. BS, broad CNA scores; Atezo+bev, atezolizumab + bevacizumab; HCC, hepatocellular carcinoma; HR, hazard ratio; LOH, loss of heterozygosity; OS, overall survival; PFS, progression-free survival; TME, tumour microenvironment; UMAP, uniform manifold approximation and projection; WES, whole-exome sequencing.

Immunosuppressive myeloid cells and stromal populations contribute to primary resistance to atezo+bev

Next, we explored mechanisms associated with primary resistance to atezo+bev. Using the expression data of all upregulated genes comprising the 21 specific scRNAseq-derived HCC signatures, we trained a logistic regression-based machine learning prediction algorithm to discriminate responders from non-responders to atezo+bev (see supplementary methods for details). The integrated model discriminated atezo+bev responders

with an accuracy of 93% (95% CI 0.89-0.96) and 82% (95% CI 0.66-0.92) in the training/test and validation cohorts (*i.e.* the external and in-house RNAseq cohorts), respectively, outperforming previously reported molecular correlates of atezo+bev response (Fig. S10A).

Out of 686 unique genes used as input, 229 genes were retained as most informative (Fig. S10B). Genes associated with known anti-tumoural immune cell types (*e.g.* CD16+ monocytes) were linked to response to atezo+bev, while genes linked to pro-tumoural, immunosuppressive cell types (*e.g.* CD14+ monocytes and TREM2+ macrophages) were predominantly linked to resistance (Fig. S11A). Conversely, genes composing the fibroblast, endothelial cell or cancer cell signatures did not exhibit a preferential association with response or resistance to atezo+bev, with a similar proportion of genes from these signatures linked to both response and resistance to the combination (Fig. S10B). Using pathway analysis, we found that genes within the fibroblast signature associated with primary resistance (n = 10) were related to Notch and TGF-β signalling (Fig. S11B). Similarly, within the endothelial gene signature, the 19 genes linked to resistance to atezo+bev were related to TGF-β signalling, while the 12 genes linked to response were related to nitric oxide-mediated signalling (Fig. S11C), previously associated with bevacizumab efficacy in other tumour types.[36,37] Of note, genes within the cancer cell signature were linked to metabolic hepatic cell processes regardless of their contribution to response or resistance (Fig. S11D). Overall, these data suggest that there are likely distinct subtypes of intra-tumoural endothelial cells or tumour-associated fibroblasts that may play distinct roles in the context of atezo+bev treatment. Additionally, our findings point toward the contribution of stromal-related signalling pathways (Notch and TGF-β) and specific immunosuppressive myeloid populations (CD14+ monocytes and TREM2+ macrophages) to resistance to atezo+bev in advanced HCC.

Finally, we investigated the association between the identified resistance-related features and disease progression (PD) following atezo+bev treatment. Progressors presented a mOS of 7.96 months, contrasting starkly with patients achieving SD (mOS of 18.51 months, p <0.0001; Fig. S12). Moreover, in the external RNASeq cohort, 24% of patients with PD upon atezo+bev presented with *ImmunePos* tumours at baseline. Strikingly, *ImmunePos* tumours from progressors were significantly enriched in gene signatures capturing both CD14+

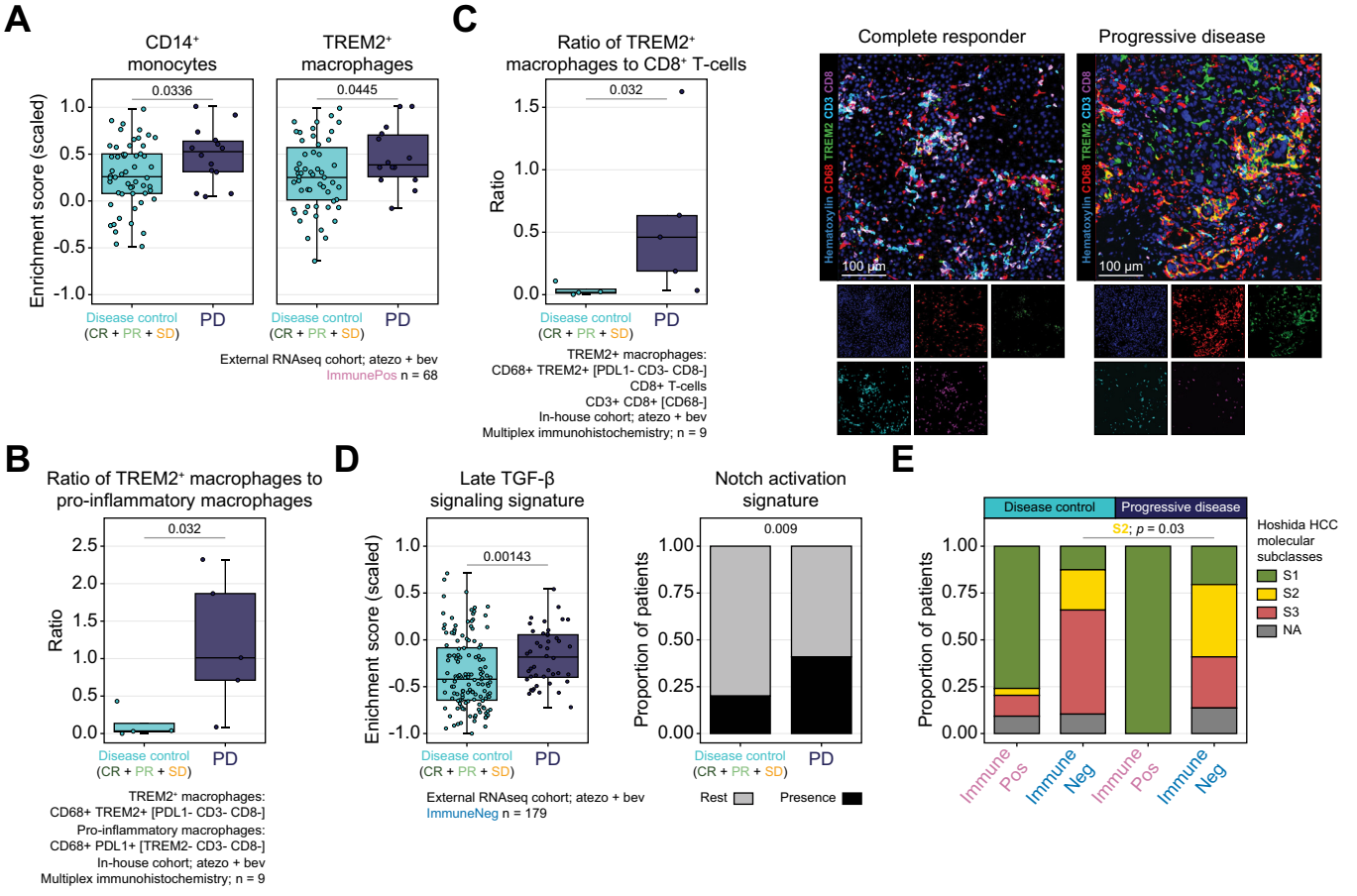

Fig. 6. Determinants of primary resistance to atezo+bev in advanced HCC. (A) Boxplot depicting the enrichment of CD14+ monocytes and TREM2+ macrophages in patients with *ImmunePos* tumours with progressive disease *vs.* disease control after atezo+bev. (B,C) Boxplot depicting the ratio of TREM2+ macrophages to pro-inflammatory macrophages (B) and to CD8+ T cells (C), with representative images. (D) Boxplot depicting the enrichment of the Late TGF-β signature (*left*) and barplot showing the frequency of Notch pathway activation (*right*) in patients with *ImmuneNeg* tumours with progressive disease *vs.* disease control after atezo+bev. (E) Barplot displaying the frequency of S1, S2 or S3-classified tumours amongst patients who showed progressive disease *vs.* disease control after atezo+bev. Statistics: A-E: Student's *t* test, Welch's *t*-test or Wilcoxon rank sum test or Fisher's exact test, as appropriate. Atezo+bev, atezolizumab + bevacizumab; CR, complete response; HCC, hepatocellular carcinoma; PD, progressive disease; PFS, progression-free survival; PR, partial response; SD, stable disease.

monocytes and TREM2+ macrophages when compared to *ImmunePos* patients who achieved disease control (DC; p = 0.034 and p = 0.045; Fig. 6A). Supporting these observations, multiplex immunohistochemistry revealed a significantly higher ratio of TREM2+ macrophages to pro-inflammatory macrophages or to CD8+ T cells in patients with PD *vs.* DC upon atezo+bev (Fig. 6B,C).

Next, we explored whether *ImmuneNeg* progressors showed an increase in stromal-related signalling pathways such as TGF-β or Notch. Indeed, *ImmuneNeg* patients with PD were characterised by a significant increase in the so-called "late TGF-β signature" – known to be associated with TGF-β oncogenic effects in HCC[38] – when compared with *ImmuneNeg* patients with DC (p = 0.001; Fig. 6D, *left*). Moreover,

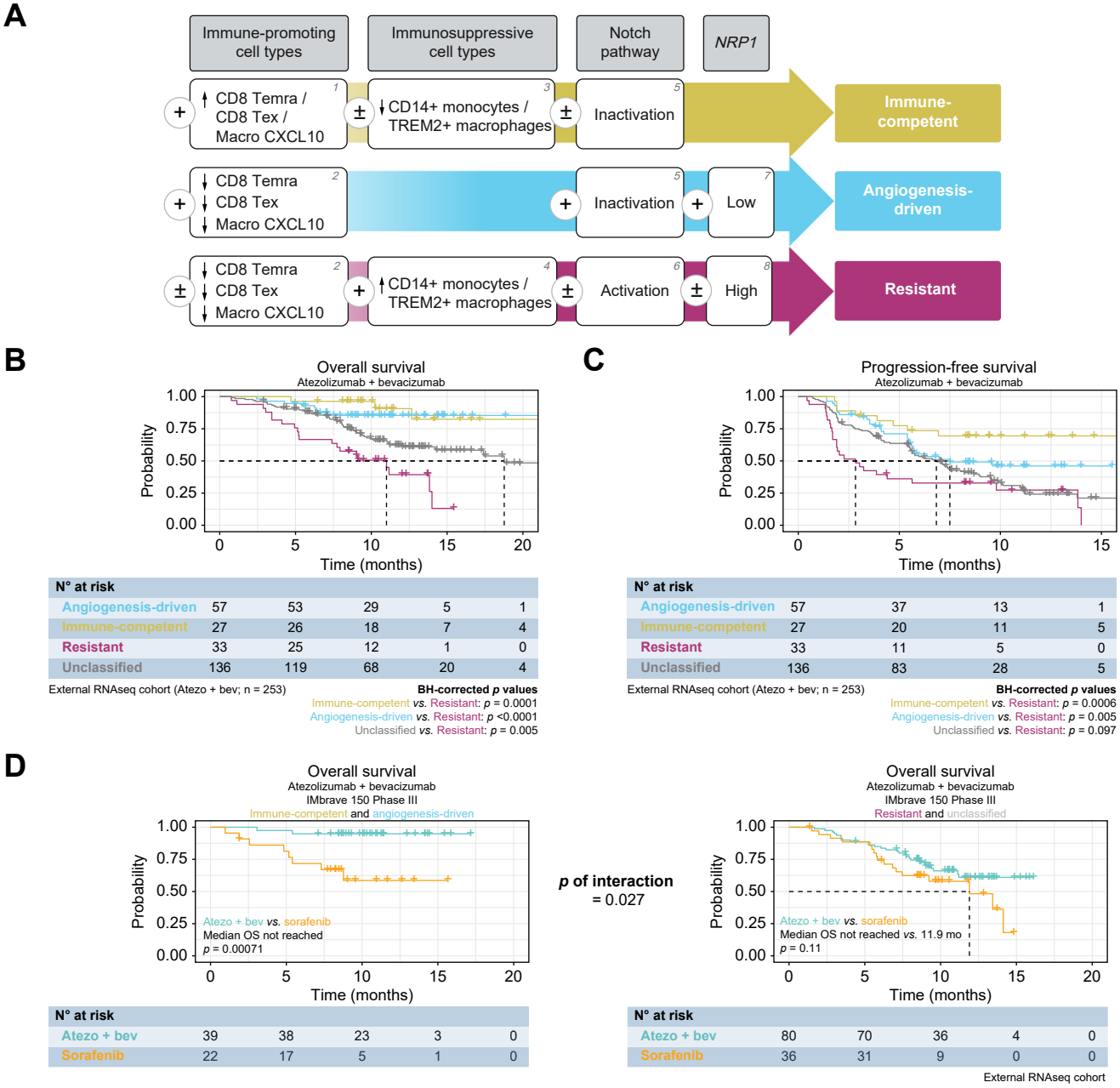

Fig. 7. Molecular subsets determine clinical outcomes to atezo+bev in advanced HCC. (A) Flowchart summarising the classification criteria into the distinct molecular subsets, defined by: [1]Presence of CD8 Temra, CD8 Tex, or Macro CXCL10; [2]Absence of CD8 Temra, CD8 Tex or Macro CXCL10; [3]Absence of CD14+ monocytes or TREM2+ macrophages; [4]Presence of CD14+ monocytes or TREM2+ macrophages; Absence[5] or presence[6] of Notch; Decreased *NRP1* expression[7] or not.[8] (B,C) Kaplan-Meier curves depicting OS and PFS of atezo+bev-treated patients (n = 253) according to molecular subset. (D) Kaplan-Meier curves depicting OS in the IMbrave150 study (n = 177) stratified according to "*Immune-competent*" and "*Angiogenesis-driven*" (*left*) or "*Unclassified*" and "*Resistant*" (*right*) classification. Statistics: B–C: log-rank test with Benjamini-Hochberg adjustment. D: log-rank test. *P* of interaction calculated using a Cox proportional hazards model. Atezo+bev, atezolizumab + bevacizumab; HCC, hepatocellular carcinoma; OS, overall survival; PFS, progression-free survival.

ImmuneNeg patients with PD exhibited an enrichment in Notch pathway activation,[22] compared to *ImmuneNeg* patients with DC (p = 0.009; Fig. 6D, *right*). In addition, these patients also displayed a higher presence of the progenitor-like Hoshida S2 subclass[39] (p = 0.03; Fig. 6E).

Consistently, tumours from the syngeneic Hep53.4 model showing anti-PDL1 + anti-VEGFA resistance (Fig. S8) were classified as Notch-active, exhibited high levels of NRP1, and were enriched in CD14+ monocytes and TREM2+ macrophages, both in mice treated with vehicle and the combination of anti-PDL1 + anti-VEGFA (Fig. S13).

Taken together, our findings identify potential factors contributing to upfront progressive disease upon atezo+bev treatment in advanced HCC, including the presence of immunosuppressive immune cell populations, such as TREM2+ macrophages and CD14+ monocytes, as well as a stromal contribution stemming from Notch activation and TGF-β signalling. These insights offer valuable implications for understanding the intricate mechanisms underlying resistance to atezo+bev in advanced HCC.

Defining molecular subsets that determine clinical benefit and primary resistance to atezo+bev in advanced HCC

Finally, we aimed to integrate our findings related to the proposed mechanisms of response and resistance to atezo+bev to define subgroups that correlate with therapeutic benefit. To this end, atezo+bev-treated patients from the external RNAseq cohort were categorized into three main molecular subsets: *"Immune-competent"*, "*Angiogenesis-driven*" and *"Resistant"* (Fig. 7A; see supplementary methods for details) based on i) the presence or absence of immune-promoting *vs.* immunosuppressive cell types, ii) Notch pathway activation and iii) intratumoural *NRP1* expression levels. Importantly, patients belonging to the *"Immune-competent"* and *"Angiogenesis-driven"* groups had a significantly longer OS upon atezo+bev treatment compared to those defined as *"Resistant"* (mOS; not reached *vs.* 11 months; p = 0.0001 and p <0.0001 respectively; Fig. 7B). These observations were validated when splitting the cohort into patients receiving atezo+bev in the GO30140 phase Ib (n = 134) *vs.* the IMbrave150 phase III (n = 119) trials (Fig. S14A and B). Of note, the "*Resistant*" patient group was also associated with a significantly shorter OS when compared to "*Unclassified*" patients (mOS; 11 *vs.* 18.8 months; p = 0.005; Fig. 7B). Similarly, both the *"Immune-competent"* and *"Angiogenesis-driven"* subgroups presented with significantly longer PFS compared to *"Resistant"* patients (mPFS; not reached *vs.* 2.8 months; p = 0.0006 and 7.5 *vs.* 2.8 months; p = 0.005, respectively; Fig. 7C).

Furthermore, patients from the IMbrave150 trial classified as *"Immune-competent"* or *"Angiogenesis-driven"* had significantly longer OS upon atezo+bev compared to sorafenib treatment (p = 0.0007; Fig. 7D), as opposed to *"Resistant"* or *"Unclassified"* groups. In short, the combined "*Immune-competent*" and "*Angiogenesis-driven*" molecular subgroups demonstrated a significant capacity to predict clinical benefit to atezo+bev (p of interaction = 0.027; Fig. 7D).

Altogether, we identified two distinct molecular subsets associated with clinical benefit upon atezo+bev treatment in advanced HCC, each driven by an immune- or angiogenesis-related mechanism. Additionally, we identified the molecular landscape of patients presenting with the poorest survival outcomes after atezo+bev. These findings offer potential applications to molecularly stratify patients based on the efficacy of immunotherapy and anti-angiogenic treatments in advanced HCC.

Discussion

Our study is the first to use gene signatures derived from scRNAseq data to accurately identify 21 cell types present in the pre-treatment TME of advanced HCC. We demonstrate their use as invaluable tools to gain insights into the underlying biological mechanisms that drive treatment response and underline their potential clinical application, effectively bridging the gap between scRNAseq and RNAseq data. In doing so, we describe two distinct molecular-based types of response to atezo+bev treatment and define traits characterising primary resistance.

First, approximately 40% of responding tumours were characterised by a pre-existing anti-tumoural immunity defined by the infiltration of CD8+ effector T cells and pro-inflammatory CXCL10+ macrophages, previously related to atezo+bev response.[6,17] Additionally, these tumours presented an inflamed microenvironment with molecular features of ICI monotherapy response,[10–13,25–29] suggesting their susceptibility to the immune-activating effect of atezolizumab.

Conversely, the remaining 60% of tumours responding to atezo+bev displayed similar immune infiltration levels to non-responders but were characterised by genomic instability features, including *TP53* alterations, previously associated with anti-VEGF response.[33] This subgroup of tumours also showed *NRP1* downregulation, a characteristic previously reported as a biomarker of response to bevacizumab monotherapy[34] and associated with longer PFS with bevacizumab treatment in other cancers.[40] Preclinical studies have shown that blocking *NRP1* function renders blood vessels more susceptible to anti-VEGF therapy by means of a vascular remodelling process that results in reduced pericyte-vessel associations.[41] Consistently, in our data, *NRP1* was mostly expressed in endothelial cells and pericytes. These findings support the notion that clinical benefit in this subgroup of tumours may result from the anti-angiogenic effect of bevacizumab.

Whether a subset of responders may benefit from the synergistic effect of both mechanisms is certainly possible, though controversial in a setting where we have phase III data for both ICI monotherapy, anti-VEGFA monotherapy and their combination.[42] In theory, anti-angiogenic drugs such as bevacizumab have the capacity to counteract immunosuppressive pathways and restore a functional vasculature to i) improve T-cell recruitment into the tumour and ii) increase the bioavailability of anti-PDL1 within the tumour.[6,43,44] In this case, the resulting therapeutic effect may only be visible within the tumour after treatment, a phenomenon that we cannot capture in the absence of on-treatment tumour samples.

Next, we explored the immune cells and pathway-related mechanisms characterising atezo+bev progressors. We found that the intra-tumoural stromal compartment exhibits unique features associating TGF-β and Notch signalling with resistance to atezo+bev, consistent with previous reports linking these pathways to resistance against anti-PDL1[45] or anti-VEGFA in other cancers[46] and HCC.[47]

Overall, most atezo+bev progressors (~75%) exhibited low levels of immune infiltration by CD8+ effector T cells or pro-inflammatory CXCL10+ macrophages. These patients were enriched in Notch signalling and exhibited progenitor-like traits, aligning with previous findings linking high *AFP* and *GPC3* levels to atezo+bev resistance.[6] Surprisingly, ~25% of progressors were infiltrated by CD8+ effector T cells or pro-inflammatory CXCL10+ macrophages, suggesting the presence of a pre-existing anti-tumoural immunity. Notably, these tumours were also highly infiltrated by two immunosuppressive myeloid cell types, namely TREM2+ macrophages and their precursor, CD14+ monocytes,[48] previously associated with immunotherapy resistance.[49] Moreover, TREM2+ macrophages have been associated with an immunosuppressive role in lung cancer,[50] and have been found to suppress CD8+ T-cell activity and promote anti-PDL1 resistance in patients with HCC after transarterial chemoembolisation.[51] In short, a subset of progressors display a pre-existing immune response that is likely overshadowed by an immunosuppressive myeloid component that contributes to therapeutic inefficacy of atezo+bev in these patients.

Finally, by integrating the distinct determinants of response and resistance to atezo+bev, we provide a molecular-based classification comprising three subsets of patients: two subtypes of patients associated with good outcome ("*Immune-competent*" and "*Angiogenesis-driven*"), and a "*Resistant*" subset associated with poor outcome (Fig. 7). Importantly, both the "*Immune-competent*" and "*Angiogenesis-driven*" subgroups were associated with significantly improved OS upon atezo+bev treatment, with a probability of 80% survival at 20 months (median not reached). In addition, both molecular subgroups were independently associated with improved OS and PFS after atezo+bev when compared to the "*Resistant*" subgroup, which had significantly worse OS (mOS: 11 months) compared to all other patient groups. In short, we defined novel molecular subsets predictive of clinical outcomes to atezo+bev in advanced HCC using widely accessible transcriptomic analysis, which may help guide clinical decision making in HCC in the future.

The main limitation of our study is that to ensure data consistency across cohorts, only samples taken within 12 months of treatment initiation were included, resulting in a limited sample size in the in-house RNAseq cohort. Furthermore, our study identifies several factors associated with response or resistance to atezo+bev, but to demonstrate a causal relationship further mechanistic validation experiments are required. Additionally, despite the significant predictive capacity of the proposed molecular subsets to discriminate atezo+bev clinical outcomes, a large proportion of patients remain unclassified. Finally, the limited availability of detailed clinical information from the external RNAseq cohort constrained our ability to conduct a multivariate analysis or assess the potential influence of underlying liver aetiology on the response patterns to atezo+bev observed in this study.

In conclusion, we leveraged the resolution of scRNAseq to derive gene signatures and unravel determinants of atezo+bev response and resistance. By integrating our findings, we uncovered both an "*Immune-competent*" and an "*Angiogenesis-driven*" phenotype that derive clinical benefit from atezo+bev, likely due to distinct biological mechanisms. Furthermore, we identified a "*Resistant*" subset associated with poor survival outcomes upon atezo+bev treatment in advanced HCC.

Affiliations

[1]*Digestive Oncology, Department of Gastroenterology, University Hospitals Leuven, Leuven, Belgium;* [2]*Laboratory of Clinical Digestive Oncology, Department of Oncology, KU Leuven, Leuven, Belgium;* [3]*Laboratory for Translational Genetics, Department of Human Genetics, KU Leuven, Leuven, Belgium;* [4]*VIB Centre for Cancer Biology, Leuven, Belgium;* [5]*Mount Sinai Liver Cancer Program (Divisions of Liver Diseases, Department of Hematology/Oncology, Department of Medicine), Tisch Cancer Institute, Icahn School of Medicine at Mount Sinai, New York, USA;* [6]*Liver Cancer Translational Research Group, Institut d'Investigacions Biomèdiques August Pi i Sunyer (IDIBAPS), Hospital Clínic, Universitat de Barcelona, Barcelona, Catalonia, Spain;* [7]*Radiology Department, University Hospitals Leuven, Leuven, Belgium;* [8]*Laboratory of Translational MRI, Department of Imaging and Pathology, KU Leuven, Leuven, Belgium;* [9]*Pathology Department and Molecular Biology Core, Hospital Clínic of Barcelona, Barcelona, Spain;* [10]*Institut de Génomique Fonctionnelle, Univ. Montpellier, CNRS, INSERM, Montpellier, France;* [11]*Department of Surgery, Campus Charité Mitte and Campus Virchow-Klinikum, Charité-Universitätsmedizin Berlin, 13353 Berlin, Germany;* [12]*Department of Immunology and Immunotherapy, Icahn School of Medicine at Mount Sinai, New York, NY, USA;* [13]*Department of Surgery & Cancer, Imperial College London, Hammersmith Hospital, London, UK;* [14]*Department of Hepatology and Gastroenterology, Charité - Universitätsmedizin Berlin, Campus Virchow Klinikum (CVK) and Campus Charité Mitte (CCM), Berlin, Germany;* [15]*Research Department of Oncology, UCL Cancer Institute, University College London, Royal Free Hospital, London, UK;* [16]*Department of Visceral Surgery and Medicine, Inselspital, Bern University Hospital, University of Bern, Bern, Switzerland;* [17]*Department of Medicine I, University Medical Center Schleswig Holstein Campus Lübeck, Lübeck, Germany;* [18]*Hepatopancreatobiliary Multidisciplinary Team, Newcastle upon Tyne NHS Foundation Trust, Freeman Hospital, Newcastle upon Tyne, UK;* [19]*Newcastle University Translational and Clinical Research Institute and Newcastle University Centre for Cancer, Medical School, Framlington Place, Newcastle Upon Tyne, NE2 4HH, UK;* [20]*Department of Medical Oncology, Centre Eugène Marquis, Rennes, France;* [21]*Department of Gastroenterology, University Liver and Cancer Centre, Frankfurt, Germany;* [22]*Department of Medicine I, University Medical Center of the Johannes-Gutenberg University, Mainz, Germany;* [23]*Liver Unit, Hospital Universitari Vall d'Hebron, Vall d'Hebron Barcelona Hospital Campus, Barcelona, Spain;* [24]*Liver Diseases Research Group, Vall d'Hebron Institute of Research (VHIR), Vall d'Hebron Barcelona Hospital Campus, Barcelona, Spain;* [25]*CIBERehd, Universitat Autònoma de Barcelona, Barcelona, Spain;* [26]*Department of Medical Oncology, Cancer Biomarkers Research Group, Hospital Universitari Arnau de Vilanova, IRBLleida, University of Lleida (UdL), Catalonia, Spain;* [27]*Department of Translational Medicine, Università Del Piemonte Orientale "A. Avogadro", Novara, Italy;* [28]*Division of Chronic Inflammation and Cancer, German Cancer Research Center (DKFZ), Heidelberg, Germany;* [29]*Institució Catalana de Recerca i Estudis Avançats (ICREA), Barcelona, Catalonia, 08010, Spain*

Abbreviations

Atezo+bev, atezolizumab + bevacizumab; CD4 Tn, naive CD4+ T-cells; CD4 Tcm, central memory CD4+ T-cells; CD4 Tem, effector memory CD4+ T-cells; CD4 IL17, IL17-expressing CD4+ T-cells; CD4 CXCL13, CXCL13-expressing CD4+ T-cells; CD4 Treg, regulatory CD4+ T-cells; CD8 Tn, naive CD8+ T-cells; CD8 Trm, resident memory CD8+ T-cells; CD8 Tem, effector memory CD8+ T-cells; CD8 Temra, CD45RA-expressing effector memory CD8+ T-cells; CD8 Tex, exhausted CD8+ T-cells; MAIT, mucosal-associated invariant T-cells; GammaDelta, gamma-delta T-cells; NK cytotoxic, cytotoxic natural killer cells; NK resting, resting natural killer cells; cDC1, type 1 conventional dendritic cells; cDC2, type 2 conventional dendritic cells; pDC, plasmacytoid dendritic cells; mregDC, mature regulatory dendritic cells; Mono CD14, CD14-expressing monocytes; Mono CD16, CD16-expressing monocytes; Macro CCR2, CCR2-expressing macrophages; Macro CX3CR1, CX3CR1-expressing macrophages; Macro CXCL10, CXLC10-expressing macrophages; Macro SPP1, SPP1-expressing macrophages; Macro FOLR2, FOLR2-expessing macrophages; Macro TREM2, TREM2-expressing macrophages; Macro MT1G, MT1G-expressing macrophages; Macro FTL, FTL-expressing macrophages; DC, disease control; DEG, differentially expressed gene; HCC, hepatocellular carcinoma; ICI, immune checkpoint inhibitor; NRP1, neuropilin-1; OS, overall survival; PD, progressive disease; PFS,

progression-free survival; RNAseq, bulk RNA sequencing; scRNAseq, single-cell RNA sequencing; SD, stable disease; TME, tumour microenvironment.

Financial support

SC was supported by a strategic basic research fellowship from Research Foundation— Flanders (FWO; 1S95221N) and a post-doctoral fellowship from the Belgian American Educational Foundation (BAEF). MPG was supported by a pre-doctoral grant from the Spanish National Health Institute (MICINN, PRE2020-094716) and a mobility grant from "Fundació Universitària Agustí Pedro i Pons". REF was supported by a predoctoral grant from the Spanish National Health Institute (MCINN; BES-2017-081286) and a mobility grant from "Fundació Universitària Agustí Pedro i Pons". UB was supported by the EILF-EASL Juan Rodés PhD Studentship from the European Association for the Study of the Liver (EASL) and the EASL International Liver Foundation (EILF). RP is supported by the Fundació de Recerca Clínic Barcelona - IDIBAPS and by a grant from the Spanish National Health Institute (MICINN, PID2022-139365OB-I00, funded by MICIU/AEI/10.13039/501100011033 and FEDER). JAF was supported by a doctoral training grant from the University of Barcelona (PREDOCS-UB 2020) and by the "Societat Catalana de Digestologia" mobility grant. JP was supported by a PERIS ICT-Suport grant from the "Departament de Salut de la Generalitat de Catalunya" (SLT017/20/000206). AM was supported by the Generalitat de Catalunya with a FI-SDUR fellowship (2021 FISDU 00338) from AGAUR. JHP was supported by the predoctoral grant "Ayudas para la Formación de Profesorado Universitario (FPU)" (FPU21/03361) and a mobility grant from "Fundació Universitària Agustí Pedro i Pons". MZ was funded by the Deutsche Forschungsgemeinschaft (DFG, German Research Foundation; 531006414). AD is supported by the National Institute for Health Research (NIHR) Imperial BRC, by grant funding from the European Association for the Study of the Liver (2021 Andrew Burroughs Fellowship) and from Cancer Research UK (RCCPDB- Nov21/100008). HLR is supported by Cancer Research UK (CRUK) programme grant C18342/A23390, Accelerator award C9380/A26813, the CRUK Newcastle Centre CTRQQR-2021\100003; the NIHR Newcastle Biomedical Research Centre awarded to the Newcastle upon Tyne Hospitals NHS Foundation Trust and Newcastle University (grant ref: 570556) and the European Commission (Horizon Europe-Mission Cancer, THRIVE, Ref. 101136622). RM acknowledges the support from ISCIII (PI21/01619 research project and Juan Rodés contract), SEOM (research project), TTD (research project) and Fundación MERCK Salud (research project). SG was partially supported by NIH grants CA224319, DK124165, CA234212, and CA196521. DJP is supported by grant funding from the Wellcome Trust Strategic Fund (PS3416), the Associazione Italiana per la Ricerca sul Cancro (AIRC MFAG 25697) and acknowledges grant support from the Cancer Treatment and Research Trust (CTRT), the Foundation for Liver Research and infrastructural support by the Imperial Experimental Cancer Medicine Centre and the NIHR Imperial Biomedical Research Centre. The views expressed are those of the authors and not necessarily those of the NHS, the NIHR, or the Department of Health and Social Care. DL was supported by an ERC Advanced Grant (101055422) and a KU Leuven Internal Fund (C14/18/092). JML is supported by grants from European Commission (Horizon Europe-Mission Cancer, THRIVE, Ref. 101136622), the NIH (R01-CA273932-01, R01DK56621 and R01DK128289); Samuel Waxman Cancer Research Foundation; the Spanish National Health Institute (MICINN, PID2022-139365OB-I00, funded by MICIU/AEI/10.13039/501100011033 and FEDER); Cancer Research UK (CRUK), Fondazione AIRC per la Ricerca sul Cancro and Fundación Científica de la Asociación Española Contra el Cáncer (FAECC) (Accelerator Award, HUNTER, Ref. C9380/A26813); "la Caixa" Foundation under agreement LCF/PR/SP23/52950009; Fundación Científica de la Asociación Española Contra el Cáncer (FAECC; Proyectos Generales, Ref. PRYGN223117LLOV; Reto AECC 70% Supervivencia: Ref. RETOS245779LLOV; and Programa de Excelencia, EPAEC246711CLIN) and the Generalitat de Catalunya/AGAUR (2021 SGR 01347).

Conflict of interest

AD received educational support for congress attendance and consultancy fees from Roche, and speaker fees from Roche, AstraZeneca, Eisai, and Chugai. FFo has received honoraria for lectures from AstraZeneca, Lilly, MSD, Pfizer and Roche. He has served as advisory board member to AstraZeneca, BMS, Eisai and Roche and has received travel support from Merck KGaA and Servier. RM has received consulting and lecture fees from Servier, Roche and Bristol Myers Squibb and travel and education funding from MSD, Eli Lilly, Bayer, Roche, Astrazeneca. SG reports other research funding from Boehringer Ingelheim, Bristol-Myers Squibb, Celgene, Genentech, Regeneron, and Takeda not related to this study. SG is a named co-inventor on an issued patent for MICSSS, a multiplex immunohistochemistry to characterise tumours and treatment responses. The technology is filed through Icahn School of Medicine at Mount Sinai (ISMMS) and is currently unlicensed. AV has received consulting fees from FirstWorld, Natera, Pioneering Medicine and Genentech; advisory board fees from BMS, Roche, Astra Zeneca, Eisai, and NGM Pharmaceuticals; and research support from Eisai. He has stock options from Espervita. JML reports research support from Eisai Inc and Bayer Pharmaceuticals, consultancy/sponsored lectures from Eisai Inc., Merck, Roche, Genentech, AstraZeneca, Bayer Pharmaceuticals, Abbvie, Sanofi, Moderna, Glycotest and Exelixis, and Data Safety Monitoring Board for Industry or Commercial Enterprise from Bristol Myers Squibb. The remaining authors have no conflicts of interest to declare.

Please refer to the accompanying ICMJE disclosure forms for further details.

Authors' contributions

JD and JML designed and jointly supervised the study, with help from DL and AV. Clinical samples were established and clinically annotated by SC, MPG, MZ, VV, PKH, AD, RMoh, TM, AL, JUM, HLR, JE, FF, JT, PG, FFo, BM, RM, DJP, CV, EVC, JD and JML. Data analysis was performed by SC, MPG and REF with substantial help from GP. REF designed the integrative model and created PredictOR with contributions from SC and MPG. CM contributed to the pathological characterisation of tumour samples. LB contributed to the analysis of genomic data. UB, JP, AM, and JHP were involved in sample processing including RNA isolation. IF, GI, EGK and SG contributed to the multiplexed immunohistochemical (IHC) consecutive staining on single slide (MICSSS) analysis. RP, AGO, JAF, MH, CV and EVC provided scientific input and contributed to critical data interpretation. The manuscript was written by SC and MPG with substantial contribution from REF and under supervision of JD and JML. All authors read or provided comments on the manuscript.

Data availability statement

RNA sequencing data of the Inhouse RNAseq Cohort, generated for the purpose of this study, have been deposited at the European Genome phenome Archive (EGA; https://ega-archive.org) with accession number EGAD50000001227.

Acknowledgments

We thank Thomas van Brussel, Rogier Schepers and Evy Vanderheyden for all hands-on work related to single-cell experiments. We thank Maria Esteve-García for her support with RNA extractions. We are indebted to the Cytometry and Cell Sorting Core Facility of the Institut d'Investigacions Biomèdiques August Pi i Sunyer (IDIBAPS), particularly Cristina López, for excellent flow cytometry technical assistance. This work was supported in part through the computational and data resources and staff expertise provided by Scientific Computing and Data at the Icahn School of Medicine at Mount Sinai and supported by the Clinical and Translational Science Awards (CTSA) grant UL1TR004419 from the National Center for Advancing Translational Sciences. Research reported in this publication was also supported by the Office of Research Infrastructure of the National Institutes of Health under award number S10OD026880 and S10OD030463. The content is solely the responsibility of the authors and does not necessarily represent the official views of the National Institutes of Health. In addition, the study was in part developed in the Centre Esther Koplowitz from IDIBAPS/CERCA Programme/Generalitat de Catalunya.

Supplementary data

Supplementary data to this article can be found online at https://doi.org/10.1016/j.jhep.2024.12.016.

References

Author names in bold designate shared co-first authorship

[1] Sung, Ferlay, Siegel, et al. Global cancer statistics 2020: GLOBOCAN estimates of incidence and mortality worldwide for 36 cancers in 185 Countries. CA Cancer J Clin 2021;71:209–249.
[2] Llovet, Pinyol, Kelley, et al. Molecular pathogenesis and systemic therapies for hepatocellular carcinoma. Nat Cancer 2022;3:386–401.
[3] Llovet, Ricci, Mazzaferro, et al. Sorafenib in advanced hepatocellular carcinoma. NEJM 2008;359:378–390.
[4] Finn, Qin, Ikeda, et al. Atezolizumab plus bevacizumab in unresectable hepatocellular carcinoma. NEJM 2020;382:1894–1905.
[5] Cheng, Qin, Ikeda, et al. Updated efficacy and safety data from IMbrave150: atezolizumab plus bevacizumab vs. sorafenib for unresectable hepatocellular carcinoma. J Hepatol 2022;76:862–873.

[6] Zhu, Abbas, de Galarreta, et al. Molecular correlates of clinical response and resistance to atezolizumab in combination with bevacizumab in advanced hepatocellular carcinoma. Nat Med 2022;28:1599–1611.
[7] Cappuyns, Llovet. Combination therapies for advanced hepatocellular carcinoma: biomarkers and unmet needs. CCR 2022;28:3405–3407.
[8] Greten, Villanueva, Korangy, et al. Biomarkers for immunotherapy of hepatocellular carcinoma. Nat Rev Clin Oncol 2023;20:780–798.
[9] Llovet, Castet, Heikenwalder, et al. Immunotherapies for hepatocellular carcinoma. Nat Rev Clin Oncol 2022;19:151–172.
[10] Haber, Castet, Torres-Martin, et al. Molecular markers of response to anti-PD1 therapy in advanced hepatocellular carcinoma. Gastroenterology 2022:S0016–S5085. 01039–3.
[11] Sangro, Melero, Wadhawan, et al. Association of inflammatory biomarkers with clinical outcomes in nivolumab-treated patients with advanced hepatocellular carcinoma. J Hepatol 2020;73:1460–1469.
[12] Neely, Yao, Kudo, et al. Genomic and transcriptomic analyses related to the clinical efficacy of first-line nivolumab in advanced hepatocellular carcinoma from the phase 3 CheckMate 459 trial. AACR Annual Meeting; 2022. MS.CL11.02.
[13] Spranger, Bao, Gajewski. Melanoma-intrinsic β-catenin signalling prevents anti-tumour immunity. Nature 2015;523:231–235.
[14] **Montironi**, **Castet**, **Haber**, et al. Inflamed and non-inflamed classes of HCC: a revised immunogenomic classification. Gut 2023;72:129–140.
[15] McDermott, Huseni, Atkins, et al. Clinical activity and molecular correlates of response to atezolizumab alone or in combination with bevacizumab *vs.* sunitinib in renal cell carcinoma. Nat Med 2018;24:749–757.
[16] Lui, Xun, Ma, et al. Identification of a tumour immune barrier in the HCC microenvironment that determines the efficacy of immunotherapy. J Hepatol 2023;78:770–782.
[17] Cappuyns, Philips, Vandecaveye, et al. PD-1- CD45RA+ effector-memory CD8 T cells and CXCL10+ macrophages are associated with response to atezolizumab plus bevacizumab in advanced hepatocellular carcinoma. Nat Commun 2023;14:7825.
[18] Ma, Wang, Khatib, et al. Single-cell atlas of tumor cell evolution in response to therapy in hepatocellular carcinoma and intrahepatic cholangiocarcinoma. J Hepatol 2021;75:1397–1408.
[19] Llovet, Lencioni. mRECIST for HCC: performance and novel refinements. J Hepatol 2020;72:288–306.
[20] Olbrecht, Busschaert, Qian, et al. High-grade serous tubo-ovarian cancer refined with single-cell RNA sequencing: specific cell subtypes influence survival and determine molecular subtype classification. Genome Med 2021;13:1–30.
[21] **Hao**, **Hao**, Andersen-Nissen, et al. Integrated analysis of multimodal single-cell data. Cell 2021;184:3573–3587.e29.
[22] Villanueva, Alsinet, Yanger, et al. Notch signaling is activated in human hepatocellular carcinoma and induces tumor formation in mice. Gastroenterology 2012;143:1660–1669.e7.
[23] Chen, Tan, Kou, et al. Enrichr: interactive and collaborative HTML5 gene list enrichment analysis tool. BMC Bioinformatics 2013;128.
[24] Lee, Ryoo, Hsu, et al. Atezolizumab with or without bevacizumab in unresectable hepatocellular carcinoma (GO30140): an open-label, multicentre, phase 1b study. Lancet Oncol 2020;21:808–820.
[25] Fehrenbacher, Spira, Ballinger, *et al.* Atezolizumab *vs.* docetaxel for patients with previously treated non-small-cell lung cancer (POPLAR): a multicentre, open-label, phase 2 randomised controlled trial. The Lancet 387:1837–1846.
[26] Rooney, Shukla, Wu, et al. Molecular and genetic properties of tumors associated with local immune cytolytic activity. Cell 2015;160:48–61.
[27] Auslander, Zhang, Lee, et al. Robust prediction of response to immune checkpoint blockade therapy in metastatic melanoma. Nat Med 2018;24:1545–1549.
[28] Grasso, Tsoi, Onyshchenko, et al. Conserved interferon-γ signaling drives clinical response to immune checkpoint blockade therapy in melanoma. Cancer Cell 2020;38:500–515.e3.
[29] Ayers, Lunceford, Nebozhyn, et al. IFN-γ-related mRNA profile predicts clinical response to PD-1 blockade. JCI 2017;127:2930–2940.
[30] de Galarreta, Bresnahan, Molina-Sánchez, et al. β-catenin activation promotes immune escape and resistance to anti–PD-1 therapy in hepatocellular carcinoma. Cancer Discov 2019;9:1124–1141.
[31] Reich, Liefeld, Gould, et al. GenePattern 2.0. Nat Genet 2006;38:500–501.
[32] **Bassaganyas**, **Pinyol**, **Esteban-Fabró**, et al. Copy-number alteration burden differentially impacts immune profiles and molecular features of hepatocellular carcinoma. CCR 2020;26:6350–6361.
[33] Wheler, Janku, Naing, et al. TP53 alterations correlate with response to VEGF/VEGFR inhibitors: implications for targeted therapeutics. Mol Cancer Ther 2016;15:2475–2485.
[34] Lambrechts, Lenz, De Haas, et al. Markers of response for the anti-angiogenic agent bevacizumab. JCO 2013;31:1219–1230.
[35] Leclerc, Voilin, Gros, et al. Regulation of antitumour CD8 T-cell immunity and checkpoint blockade immunotherapy by Neuropilin-1. Nat Commun 2019;10:3345.
[36] Ulivi, Scarpi, Passardi, et al. eNOS polymorphisms as predictors of efficacy of bevacizumab-based chemotherapy in metastatic colorectal cancer: data from a randomised clinical trial. J Transl Med 2015;13:1–10.
[37] Muto, Takagi, Owada, et al. Serum nitric oxide as a predictive biomarker for bevacizumab in non-small cell lung cancer patients. Anticancer Res 2017;37:3169–3174.
[38] Coulouarn, Factor. Thorgeirsson. Transforming growth factor-β gene expression signature in mouse hepatocytes predicts clinical outcome in human cancer. Hepatology 2008;47:2059–2067.
[39] Hoshida, Nijman, Kobayashi, et al. Integrative transcriptome analysis reveals common molecular subclasses of human hepatocellular carcinoma. Cancer Res 2009;69:7385–7392.
[40] Van Cutsem, De Haas, Kang, et al. Bevacizumab in combination with chemotherapy as first-line therapy in advanced gastric cancer: a biomarker evaluation from the AVAGAST randomised phase III trial. JCO 2012;30:2119–2127.
[41] Pan, Chanthery, Liang, et al. Blocking neuropilin-1 function has an additive effect with anti-VEGF to inhibit tumor growth. Cancer Cell 2007;11:53–67.
[42] Hwangbo, Patterson, Dai, et al. Additivity predicts the efficacy of most approved combination therapies for advanced cancer. Nat Cancer 2023;4:1693–1704.
[43] Huinen, Huijbers, van Beijnum, et al. Anti-angiogenic agents — overcoming tumour endothelial cell anergy and improving immunotherapy outcomes. Nat Rev Clin Oncol 2021;18:527–540.
[44] Fukumura, Kloepper, Amoozgar, et al. Enhancing cancer immunotherapy using antiangiogenics: opportunities and challenges. Nat Rev Clin Oncol 2018;15:325–340.
[45] Batlle, Massagué. Transforming growth factor-β signaling in immunity and cancer. Immunity 2019;50:924–940.
[46] Negri, Crafa, Pedrazzi, et al. Strong Notch activation hinders bevacizumab efficacy in advanced colorectal cancer. Future Oncol 2015;11:3167–3174.
[47] Lindblad, Donne, Liebling, et al. NOTCH1 drives sexually dimorphic immune responses in hepatocellular carcinoma. Cancer Discov 2024. https://doi.org/10.1158/2159-8290.CD-24-1215.
[48] Zhou, Wang, Guo, et al. Integrated analysis highlights the immunosuppressive role of TREM2+ macrophages in hepatocellular carcinoma. Front Immunol 2022;13:848367.
[49] Tu, Chen, Zheng, et al. S100A9+CD14+ monocytes contribute to anti-PD-1 immunotherapy resistance in advanced hepatocellular carcinoma by attenuating T cell-mediated antitumor function. J Exp Clin Cancer Res 2024;43:72.
[50] Rodriguez, Chen, Li, et al. Targeting immunosuppressive Ly6C+ classical monocytes reverses anti-PD-1/CTLA-4 immunotherapy resistance. Front Immunol 2023;14:1161869.
[51] Tan, Fan, Liu, et al. TREM2+ macrophages suppress CD8+ T-cell infiltration after transarterial chemoembolisation in hepatocellular carcinoma. J Hepatol 2023;79:126–140.

Keywords: Advanced Hepatocellular Carcinoma; Atezolizumab and bevacizumab; Biomarkers of Response; Single-Cell RNA-Sequencing; Primary Resistance.
Received 2 February 2024; received in revised form 29 November 2024; accepted 7 December 2024; available online 19 December 2024